Supplementary Materials for:

"Comparison of geodetic slip-deficit and geologic fault slip rates reveals that variability of elastic strain accumulation and release rates on strike-slip faults is controlled by the relative structural complexity of plate-boundary fault systems"

Judith Gauriau, James F. Dolan

University of Southern California, Los Angeles, CA 90089-0740, USA

Corresponding author: Judith Gauriau (gauriau@usc.edu)

This document includes additional information on the methods used in this study, as well as Figures S1, S2 and Table S1.

1. Calculation of CoCo values

Values of the Coefficient of Complexity (CoCo) for the Haiyuan, Altyn Tagh and Kunlun faults were calculated using the Himalayan fault system database from Mohadjer et al. (2016).

The CoCo value for the Denali fault was calculated thanks to the use of the Alaskan fault system database (Koehler et al., 2011).

Our CoCo calculation follows the one detailed in Gauriau and Dolan (2021). One slight change has been brought: Instead of using slip-rate bins up to 20 mm/yr, we further slice the possible ranges into the following ones, for slip rates that are faster than 20 mm/yr: [15 – 20[; [20 – 25[, [25 – 30[and >30, for which we assign a median value for the CoCo calculation: 17, 22, 27, and 35 mm/yr respectively (see Gauriau and Dolan (2021) for complete methodology). This only aims at assigning values to fast-slipping sections that are closer to the actual slip rate, which applies to the CoCo calculation of the sites located on the Calico the Garlock and the San Jacinto faults only.

2. Remarks on the behavior of faults with intermediate CoCo values

Some faults are neither truly low-Coco nor high-CoCo, but rather fall into an intermediate area among the whole range of CoCo values. For example, the Central Denali (16) and the Altyn Tagh (18) faults exhibit intermediate CoCo values that help us define an approximate boundary low- and high-CoCo faults. As noted by Dolan & Meade (2017), the central Denali fault's long-term/large-displacement slip rate, 12.1 ± 1.7 mm/yr, averaged over 12 ky and 144 m (Matmon et al., 2006) is faster than its geodetic slip-deficit rate of 7.0 ± 0.3 mm/yr inferred from block model analysis (Elliott and Freymueller, 2020) (Table 1). The Denali fault, according to its relatively low CoCo value, would be thought to behave in a relatively constant manner, since the only major faults it might interact with are the Totschunda-Duke River fault (slipping at ~ 6 mm/yr during the Holocene, Matmon et al., 2006) and the Susitna Glacier fault (a slow-slipping thrust fault). Elsewhere along the Denali fault, the geodetic rates fall within a range of 6 to 8 mm/yr. Other slip-rate sites located more to the west exhibit slower geologic slip rate values, such as 9.4 ± 1.6 mm/yr (data point 17 in Figure 2; Matmon et al., 2006), which still is faster than the elastic strain accumulation rate, which at that location is 7.8 ± 0.3 mm/yr (Elliott and Freymueller, 2020). This geologic/geodetic rate ratio <1 for a low-CoCo fault might be explained by possible long-term post-seismic effects of the 1964 M_w 9.2 Alaska earthquake, which might add up to the ones of the 2002 Denali earthquake. Alternatively, given that the Aleutian megathrust is characterized by a flat and shallow slab (Jadamec et al., 2013), and that it

might be located less than 100 km below the Denali fault (Martin-Short et al., 2018), the interaction between the slab and the Denali fault would need to be accounted for in the CoCo calculation. This, however, is speculative since it would require three-dimensional considerations, whereas the CoCo analysis, as initially designed and used here, considers the 2D (ground surface) relationships among fault systems.

On the other hand, the Altyn Tagh fault exhibits a geologic slip rate behavior that is constant, with a slip rate of 9.4 mm/yr averaged both over 54 m and 156 m displacements (Cowgill, 2007; Cowgill et al., 2009), very close to the collocated slip-deficit geodetic rate of 9 ± 4 mm/yr (Bendick et al., 2000). Several active reverse faults parallel to the Altyn Tagh fault (Yun et al., 2020) participate in the CoCo value, which places the Altyn Tagh fault's behavior between the CoCo values of the central Denali fault (16) and the Kunlun fault (19).

3. Comparison of geodetic rates with geologic rates

Figure S1 displays the slope of each geodetic rate/geologic rate comparison, with geologic rates differentiated by the displacement over which they are averaged.

As mentioned in the main text, assuming a linear relationship between geologic slip rates and geodetic rates going through the origin, we find a scaling line with best-fit slope and 1σ confidence of 0.945 ± 0.028 for low-CoCo faults using the large-displacement geologic rates, and a scaling line with best-fit slope of 1.103 ± 0.050 for the small-displacement average geologic rates.

For the high-CoCo faults, we find a scaling line with best-fit slope of 0.696 ± 0.140 using the large-displacement geologic rates and a scaling line with best-fit slope of 0.751 ± 0.162 using the small-displacement geologic rates.

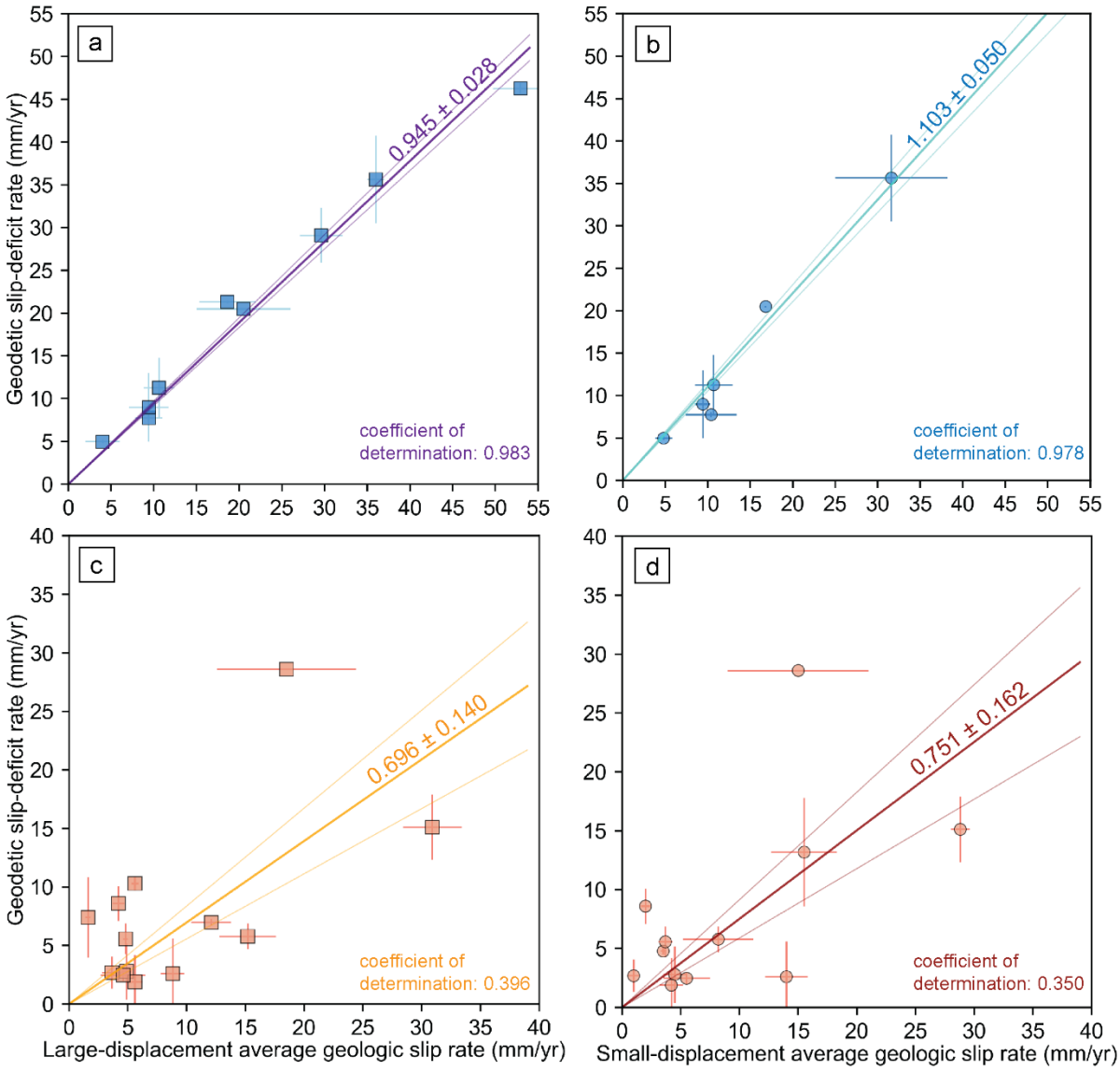

Figure S1*: Geodetic rate and geological slip rate comparisons for selected strike-slip faults.* ***(a)*** *and* ***(b)*** *for low-CoCo faults,* ***(c)*** *and* ***(d)*** *for high-CoCo faults. The dark line and the two faded lines show the linear fits with 67% confidence intervals with slopes indicated on each plot.*

4. Most recent events and recurrence intervals

The following table summarizes the available information on the studied strike-slip faults regarding their most recent event and average recurrence interval.

Table S1: *Date of most recent earthquakes that occurred on the studied strike-slip faults*

Fault	Fault section	MRE	References for MRE	Cluster of events?	Mean recurrence interval (years)	References for recurrence interval	Elapsed time since MRE (years)
Garlock	central	1545 C.E.	Dawson et al. (2003)	yes (500 yrs rec)	1000		478
San Andreas	Mojave	1857 C.E.			~100	Scharer et al. (2017)	166
San Andreas	Carrizo plain	1858 C.E.			88 ± 41	Akçiz et al. (2010)	166
San Jacinto	Claremont	1744-1850 C.E.	Onderdonk et al. (2015)	most recent cluster occurring between A.D. 1400 and A.D. 1850	156-195 (~164)	Onderdonk et al. (2015)	226
Owens Valley	northern	1872 C.E.	Beanland and Clark (1993)		3000-4100	Lee et al. (2001)	151
Calico fault	northern	0.6-2.0 ka*	Ganev et al. (2010)		~1500-2000	Ganev et al. (2010)	~600-2000
Hope	Taramakau	1800-1840 C.E.	Vermeer et al. (2022)				203
Hope	Conway	~1840 C.E.	Hatem et al. (2019)		~291	Hatem et al. (2019)	183
Hope	Hurunui	1888 C.E.	Khajavi et al. (2016)		298±88	Khajavi et al. (2016)	135
Wairau		268-1048 C.E.	Nicol and Van Dissen (2018)	onshore section could have experienced a period of increased earthquake frequency since 5600 yr BP	~1000		1365
Clarence		110-310 C.E.	Van Dissen and Nicol (2009)		~1700		1813
Awatere		1848 C.E.	Mason et al. (2006)		820–950	Mason et al. (2006)	175
Alpine		1717 C.E.	Berryman et al. (2012); De Pascale and Langridge (2012)		329		306

***Table S1** – continued*

Fault	Fault section	MRE	References for MRE	Cluster of events?	Mean recurrence interval (years)	References for recurrence interval	Elapsed time since MRE (years)
Dead Sea	Wadi Araba	1458 C.E.	Klinger et al. (2015)	seismic lull	~280	Marco et al. (1996)	565
Dead Sea	Beteiha	1202 C.E.	Wechsler et al. (2018)	past 1200 years=lull	190	Wechsler et al. (2018)	264
Yammouneh	Lebanese restraining bend	1202 C.E.	Daëron et al. (2007)		1127±135	Daëron et al. (2007)	821
Yammouneh	Missyaf (Syria)	1170 C.E.	Meghraoui et al. (2003)		550	Meghraoui et al. (2003)	853
Rachaiya-Sergaya		~1759 C.E.	Nemer et al. (2008)		1300	Gomez et al. (2003)	264
Roum		84-239 C.E.	Nemer and Meghraoui, (2006)				1861.5
Fairweather		1958 C.E.	Witter et al. (2021)				65
Queen Charlotte		2013 C.E.	Brothers et al. (2020)				10
Denali	Central	2002 C.E.	Matmon et al. (2006)				21
Denali	Western						
Altyn Tagh	Pingding (Xorxol)	1491–1741 C.E.	Yuan et al. (2018)		620±410	Yuan et al. (2018)	407
Kunlun	west	2001 C.E.	Klinger et al. (2015)		300±50	Li et al. (2005)	22
Haiyuan	Lenglongling	1540 C.E.	Jolivet et al. (2012)		1430±140	Jiang et al. (2017)	483
North Anatolian	Erzincan (east)	1939 C.E.	Kozacı et al. (2011)		685	Hartleb et al. (2006)	84
North Anatolian	Gerede (Demir Tepe)	1944 C.E.	Hubert-Ferrari et al. (2002)		250-300	Kondo et al. (2010)	79
North Anatolian	Tahtaköprü	1943 C.E.	Kozaci et al. (2011)		250-623	Okomura et al. (2003); Kondo et al. (2004)	80
North Anatolian	Ganos (Güzelköy+Cinerçik)	1912 C.E.	Meghraoui et al. (2012)		323±142	Meghraoui et al. (2012)	111
East Anatolian	Pazarcık	2023 C.E.	Barbot et al. (2023)		~772	Güvercin et al. (2022)	0.8

* a small segment of the northern section of the Calico fault ruptured in an aftershock (magnitude 5) of the Landers earthquake in 1995

5. Choice of geodetic rates

For all geodetic slip-deficit rates used in this study, we used published values collocated with geological slip-rate data.

For the North Anatolian fault, we use DeVries et al. (2017) and choose the results from their viscoelastic model by averaging the values given by the model with $\eta M = 10^{19.0}$ Pa·s, $\eta K = 10^{19.0}$ Pa·s on the one hand, and $\eta M = 10^{18.6}$ Pa·s, $\eta K = 10^{18.0}$ Pa·s on the other hand. Only the first model is given for the Ganos segment (Meghraoui et al., 2012), so we use this one only for this site.

6. Measure of the dispersion in Figure 3b

We measure the dispersion of the data points in order to illustrate the difference between data plotting in the low-CoCo region and the data plotting in the high-CoCo region in Figure 3b of the main text.

This measure accounts for the distance between each plotted datum (the ratio between the geodetic slip-deficit rate to the geologic slip rate) and the 1:1 relationship line. We want to consider a ratio a/b (where a and b are real numbers) equally as we would consider ratio b/a. To do this, we take the inverse of all ratios that are less than 1 (***case A*** in Figure S2)

We then take the distance of each point to the 1:1 ratio line. Since it is a vertical distance, it simply is the subtraction of 1 to the ratio (Euclidian distance).

This measurement accounts for the two data points for a single fault when there are two geologic slip-rate estimates (i.e., one averaged over a small displacement, and one averaged over a large displacement). In these cases, the plotted distance on Figure 3b is the sum of the two calculated distances (***case B*** in Figure S2)

To account for a potential lack of one of the geologic slip-rate estimates (i.e., whether the small-displacement geologic slip rate or the large-displacement geologic slip rate is missing), we multiply the available single distance by two (***case C*** in Figure S2).

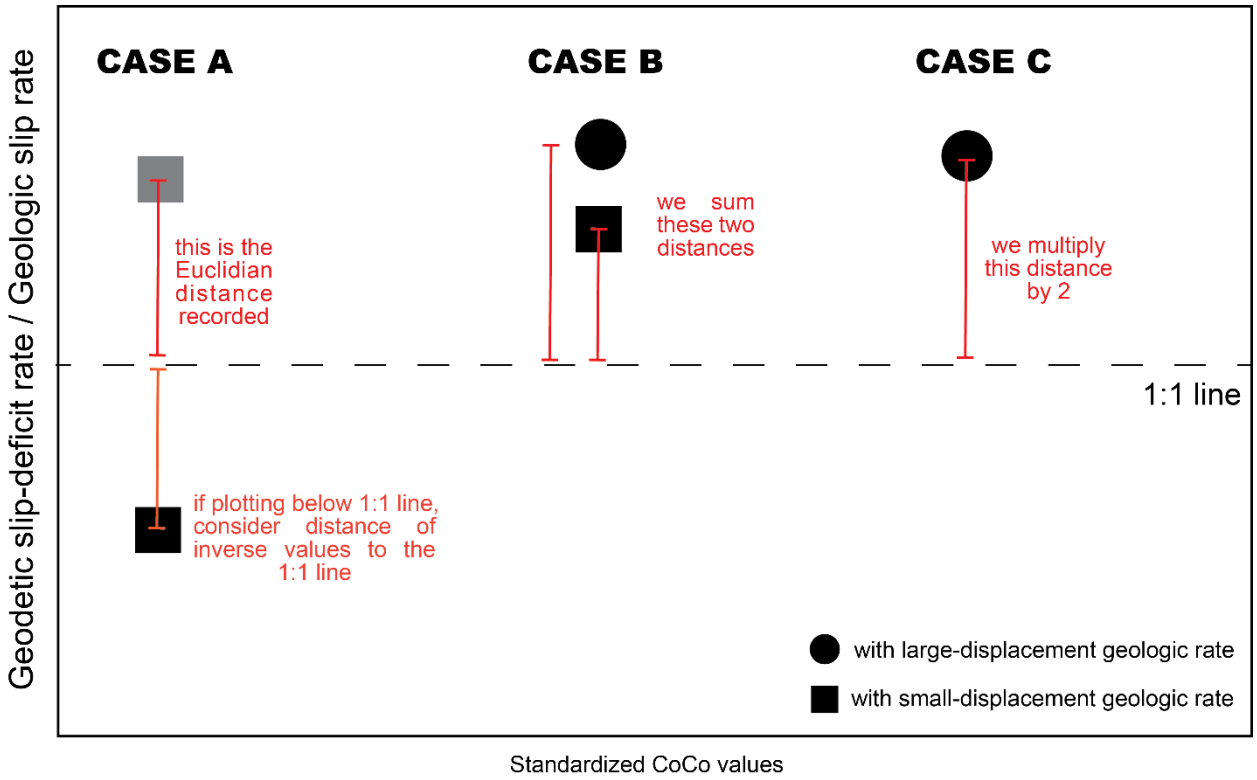

***Figure S2**: Illustration of the measurement of data dispersion shown in Figure 3b (main text).*

7. Dispersion of data points in Figure 2c

For each high-CoCo fault plotted in Figure 2c, we measured a distance from the respective data point (x = geodetic slip-deficit rate; y = small-displacement slip rate values) to the 1:1 line, which is the shortest distance from the point to the 1:1 line.

We defined fast-slipping faults as those characterized by a small-displacement slip rate that is at least 8 mm/yr, and slow-slipping faults as these characterized by a small-displacement slip rate that is less than 8 mm/yr. Using this rule, we have the following faults that fall in the fast-slipping category: the Garlock fault (1), the Mojave section of the San Andreas fault (2), the San Jacinto fault (4), the Hope fault (7) and the northern North Anatolian fault (23).

We found that for all high-CoCo faults, the average distance from the data points to the 1:1 line is 3.65 (arbitrary units). The average distance for fast-slipping high-CoCo faults only is 6.14, whereas the average distance for slow-slipping high-CoCo faults is 1.87.

References

Akçiz, S.O., Ludwig, L.G., Arrowsmith, J.R., and Zielke, O., 2010, Century-long average time intervals between earthquake ruptures of the San Andreas fault in the Carrizo Plain, California: Geology, v. 38, p. 787–790, doi:10.1130/G30995.1.

Barbot, S., Luo, H., Wang, T., Hamiel, Y., Piatibratova, O., Javed, M.T., Braitenberg, C., and Gurbuz, G., 2023, Slip distribution of the February 6, 2023 Mw 7.8 and Mw 7.6, Kahramanmaraş, Turkey earthquake sequence in the East Anatolian Fault Zone: Seismica, v. 2, doi:10.26443/seismica.v2i3.502.

Beanland, S., and Clark, M.M., 1993, Late Quaternary history of the Owens Valley fault zone, eastern California, and surface rupture associated with the 1872 earthquake: Geological Society of America, Abstracts with Programs; (United States), v. 25:5, https://www.osti.gov/biblio/5291961 (accessed December 2023).

Bendick, R., Bilham, R., Freymueller, J., Larson, K., and Yin, G., 2000, Geodetic evidence for a low slip rate in the Altyn Tagh fault system: Nature, v. 404, p. 69–72, doi:10.1038/35003555.

Berryman, K.R., Cochran, U.A., Clark, K.J., Biasi, G.P., Langridge, R.M., and Villamor, P., 2012, Major Earthquakes occur Regularly on an Isolated Plate Boundary Fault: Science, v. 336, p. 1690–1693, doi:10.1126/science.1218959.

Brothers, D.S., Miller, N.C., Barrie, J.V., Haeussler, P.J., Greene, H.G., Andrews, B.D., Zielke, O., Watt, J., and Dartnell, P., 2020, Plate boundary localization, slip-rates and rupture segmentation of the Queen Charlotte Fault based on submarine tectonic geomorphology: Earth and Planetary Science Letters, v. 530, p. 115882, doi:10.1016/j.epsl.2019.115882.

Cowgill, E., 2007, Impact of riser reconstructions on estimation of secular variation in rates of strike–slip faulting: Revisiting the Cherchen River site along the Altyn Tagh Fault, NW China: Earth and Planetary Science Letters, v. 254, p. 239–255, doi:10.1016/j.epsl.2006.09.015.

Cowgill, E., Gold, R.D., Xuanhua, C., Xiao-Feng, W., Arrowsmith, J.R., and Southon, J., 2009, Low Quaternary slip rate reconciles geodetic and geologic rates along the Altyn Tagh fault, northwestern Tibet: Geology, v. 37, p. 647–650, doi:10.1130/G25623A.1.

Daëron, M., Klinger, Y., Tapponnier, P., Elias, A., Jacques, E., and Sursock, A., 2007, 12,000-Year-Long Record of 10 to 13 Paleoearthquakes on the Yammoûneh Fault, Levant Fault System, Lebanon: Bulletin of the Seismological Society of America, v. 97, p. 749–771, doi:10.1785/0120060106.

Dawson, T.E., McGill, S.F., and Rockwell, T.K., 2003, Irregular recurrence of paleoearthquakes along the central Garlock fault near El Paso Peaks, California: Journal of Geophysical Research: Solid Earth, v. 108, doi:10.1029/2001JB001744.

De Pascale, G.P., and Langridge, R.M., 2012, New on-fault evidence for a great earthquake in A.D. 1717, central Alpine fault, New Zealand: Geology, v. 40, p. 791–794, doi:10.1130/G33363.1.

DeVries, P.M.R., Krastev, P.G., Dolan, J.F., and Meade, B.J., 2017, Viscoelastic Block Models of the North Anatolian Fault: A Unified Earthquake Cycle Representation of Pre- and Postseismic Geodetic ObservationsA Unified Earthquake Cycle Representation of Pre- and Postseismic Geodetic

Observations: Bulletin of the Seismological Society of America, v. 107, p. 403–417, doi:10.1785/0120160059.

Dolan, J.F., and Meade, B.J., 2017, A Comparison of Geodetic and Geologic Rates Prior to Large Strike-Slip Earthquakes: A Diversity of Earthquake-Cycle Behaviors? Geochemistry, Geophysics, Geosystems, v. 18, p. 4426–4436, doi:https://doi.org/10.1002/2017GC007014.

Elliott, J., and Freymueller, J.T., 2020, A Block Model of Present-Day Kinematics of Alaska and Western Canada: Journal of Geophysical Research: Solid Earth, v. 125, p. e2019JB018378, doi:10.1029/2019JB018378.

Ganev, P.N., Dolan, J.F., Blisniuk, K., Oskin, M., and Owen, L.A., 2010, Paleoseismologic evidence for multiple Holocene earthquakes on the Calico fault: Implications for earthquake clustering in the Eastern California shear zone: Lithosphere, v. 2, p. 287–298, doi:10.1130/L82.1.

Gauriau, J., and Dolan, J.F., 2021, Relative structural complexity of plate-boundary fault systems controls incremental slip-rate behavior of major strike-slip faults: Geochemistry, Geophysics, Geosystems, v. 22, doi:10.1029/2021GC009938.

Gomez, F., Meghraoui, M., Darkal, A.N., Hijazi, F., Mouty, M., Suleiman, Y., Sbeinati, R., Darawcheh, R., Al-Ghazzi, R., and Barazangi, M., 2003, Holocene faulting and earthquake recurrence along the Serghaya branch of the Dead Sea fault system in Syria and Lebanon: Geophysical Journal International, v. 153, p. 658–674, doi:10.1046/j.1365-246X.2003.01933.x.

Güvercin, S.E., Karabulut, H., Konca, A.Ö., Doğan, U., and Ergintav, S., 2022, Active seismotectonics of the East Anatolian Fault: Geophysical Journal International, v. 230, p. 50–69, doi:10.1093/gji/ggac045.

Hartleb, R.D., Dolan, J.F., and Kozaci, Ö.K., 2006, A 2500-yr-long paleoseismologic record of large, infrequent earthquakes on the North Anatolian fault at Çukurçimen, Turkey: Geological Society of America Bulletin, v. 118, p. 823–840.

Hatem, A.E., Dolan, J.F., Zinke, R.W., Van Dissen, R.J., McGuire, C.M., and Rhodes, E.J., 2019, A 2000 Yr Paleoearthquake Record along the Conway Segment of the Hope Fault: Implications for Patterns of Earthquake Occurrence in Northern South Island and Southern North Island, New Zealand: Bulletin of the Seismological Society of America, v. 109, p. 2216–2239, doi:10.1785/0120180313.

Hubert-Ferrari, A., Armijo, R., King, G.C., Meyer, B., and Barka, A., 2002, Morphology, displacement, and slip rates along the North Anatolian Fault, Turkey: Journal of geophysical research Solid Earth, v. 107, p. ETG 9-1-ETG 9-33.

Jadamec, M.A., Billen, M.I., and Roeske, S.M., 2013, Three-dimensional numerical models of flat slab subduction and the Denali fault driving deformation in south-central Alaska: Earth and Planetary Science Letters, v. 376, p. 29–42, doi:10.1016/j.epsl.2013.06.009.

Jiang, W., Han, Z., Guo, P., Zhang, J., Jiao, Q., Kang, S., and Tian, Y., 2017, Slip rate and recurrence intervals of the east Lenglongling fault constrained by morphotectonics: Tectonic implications for the northeastern Tibetan Plateau: Lithosphere, v. 9, p. 417–430, doi:10.1130/L597.1.

Jolivet, R., Lasserre, C., Doin, M.-P., Guillaso, S., Peltzer, G., Dailu, R., Sun, J., Shen, Z.-K., and Xu, X., 2012, Shallow creep on the Haiyuan Fault (Gansu, China) revealed by SAR Interferometry: Journal of Geophysical Research: Solid Earth, v. 117, doi:10.1029/2011JB008732.

Khajavi, N., Langridge, R.M., Quigley, M.C., Smart, C., Rezanejad, A., and Martín-González, F., 2016, Late Holocene rupture behavior and earthquake chronology on the Hope fault, New Zealand: GSA Bulletin, v. 128, p. 1736–1761, doi:10.1130/B31199.1.

Klinger, Y., Le Béon, M., and Al-Qaryouti, M., 2015, 5000 yr of paleoseismicity along the southern Dead Sea fault: Geophysical Journal International, v. 202, p. 313–327, doi:10.1093/gji/ggv134.

Koehler, R.D., Personius, S.F., Schwarz, D.P., Haeussler, P.J., and Seitz, G.G., 2011, A Paleoseismic study along the central Denali Fault, Chistochina Glacier area, south-central Alaska: Alaska Division of Geological & Geophysical Surveys RI 2011-1, RI 2011-1 p., doi:10.14509/22361.

Kondo, H., Özaksoy, V., and Yıldirim, C., 2010, Slip history of the 1944 Bolu-Gerede earthquake rupture along the North Anatolian fault system: Implications for recurrence behavior of multisegment earthquakes: Journal of geophysical research, v. 115, doi:10.1029/2009JB006413.

Kondo, H., Özaksoy, V., Yıldirim, C., Awata, Y., Emre, Ö., and Okomura, K., 2004, 3D trenching survey at Demir Tepe site on the 1944 earthquake rupture, North Anatolian fault system, Turkey: Seismological Research Letters, v. 75.

Kozacı, Ö.K., Dolan, J.F., Yönlü, Ö., and Hartleb, R.D., 2011, Paleoseismologic evidence for the relatively regular recurrence of infrequent, large-magnitude earthquakes on the eastern North Anatolian fault at Yaylabeli, Turkey: Lithosphere, v. 3, p. 37–54, doi:10.1130/L118.1.

Lee, J., Spencer, J., and Owen, L., 2001, Holocene slip rates along the Owens Valley fault, California: Implications for the recent evolution of the Eastern California Shear Zone: Geology, v. 29, p. 819–822, doi:10.1130/0091-7613(2001)029<0819:HSRATO>2.0.CO;2.

Li, S., Zhang, X., and Fan, J., 2005, Study on rupture zone of the M=8.1 Kunlun Mountain earthquake using fault-zone trapped waves: Acta Seismologica Sinica, v. 18, p. 43–52, doi:10.1007/s11589-005-0005-0.

Marco, S., Stein, M., Agnon, A., and Ron, H., 1996, Long-term earthquake clustering: A 50,000-year paleoseismic record in the Dead Sea Graben: Journal of Geophysical Research: Solid Earth, v. 101, p. 6179–6191, doi:10.1029/95JB01587.

Martin-Short, R., Allen, R., Bastow, I.D., Porritt, R.W., and Miller, M.S., 2018, Seismic Imaging of the Alaska Subduction Zone: Implications for Slab Geometry and Volcanism: Geochemistry, Geophysics, Geosystems, v. 19, p. 4541–4560, doi:10.1029/2018GC007962.

Mason, D.P.M., Little, T.A., and vanDissen, R.J., 2006, Refinements to the paleoseismic chronology of the eastern Awatere Fault from trenches near Upcot Saddle, Marlborough, New Zealand: New Zealand Journal of Geology and Geophysics, v. 49, p. 383–397, doi:10.1080/00288306.2006.9515175.

Matmon, A., Schwartz, D.P., Haeussler, P.J., Finkel, R., Lienkaemper, J.J., Stenner, H.D., and Dawson, TE., 2006, Denali fault slip rates and Holocene–late Pleistocene kinematics of central Alaska: Geology, v. 34, p. 645–648, doi:10.1130/G22361.1.

Meghraoui, M. et al., 2003, Evidence for 830 years of seismic quiescence from palaeoseismology, archaeoseismology and historical seismicity along the Dead Sea fault in Syria: Earth and Planetary Science Letters, v. 210, p. 35–52, doi:10.1016/S0012-821X(03)00144-4.

Meghraoui, M., Aksoy, M.E., Akyüz, H.S., Ferry, M., Dikbaş, A., and Altunel, E., 2012, Paleoseismology of the North Anatolian Fault at Güzelköy (Ganos segment, Turkey): Size and recurrence time of earthquake ruptures west of the Sea of Marmara: Geochemistry, Geophysics, Geosystems, v. 13, doi:10.1029/2011GC003960.

Mohadjer, S., Ehlers, T.A., Bendick, R., Stübner, K., and Strube, T., 2016, A Quaternary fault database for central Asia: Natural Hazards and Earth System Sciences, v. 16, p. 529–542, doi:10.5194/nhess-16-529-2016.

Nemer, T., and Meghraoui, M., 2006, Evidence of coseismic ruptures along the Roum fault (Lebanon): a possible source for the AD 1837 earthquake: Journal of Structural Geology, v. 28, p. 1483–1495, doi:10.1016/j.jsg.2006.03.038.

Nemer, T., Meghraoui, M., and Khair, K., 2008, The Rachaya-Serghaya fault system (Lebanon): Evidence of coseismic ruptures, and the AD 1759 earthquake sequence: Journal of Geophysical Research: Solid Earth, v. 113, doi:10.1029/2007JB005090.

Nicol, A., and Van Dissen, R., 2018, A 6000-year record of surface-rupturing paleoearthquakes on the Wairau Fault, New Zealand: New Zealand Journal of Geology and Geophysics, v. 61, p. 341–358, doi:10.1080/00288306.2018.1498360.

Okomura, K., Rockwell, T.K., Duman, T., Tokay, F., Kondo, H., Yıldirim, C., and Özaksoy, V., 2003, Refined Slip History of the North Anatolian Fault at Gerede on the 1944 rupture:

Onderdonk, N.W., McGill, S.F., and Rockwell, T.K., 2015, Short-term variations in slip rate and size of prehistoric earthquakes during the past 2000 years on the northern San Jacinto fault zone, a major plate-boundary structure in southern California: Lithosphere, v. 7, p. 211–234, doi:10.1130/L393.1.

Scharer, K., Weldon II, R., Biasi, G., Streig, A., and Fumal, T., 2017, Ground-rupturing earthquakes on the northern Big Bend of the San Andreas Fault, California, 800 A.D. to Present: Journal of Geophysical Research: Solid Earth, v. 122, p. 2193–2218, doi:10.1002/2016JB013606.

Van Dissen, R., and Nicol, A., 2009, Mid-late Holocene paleoseismicity of the eastern Clarence Fault, Marlborough, New Zealand: New Zealand Journal of Geology and Geophysics, v. 52, p. 195–208, doi:10.1080/00288300909509886.

Vermeer, J.L., Quigley, M.C., Langridge, R.M., Duffy, B.G., Mildon, Z.K., and Diercks, M.-L., 2022, Fault slip-rates and Coulomb stress interactions in the intersection zone of the Hope, Kelly and Alpine Faults, South Island, New Zealand: Tectonophysics, v. 843, p. 229593, doi:10.1016/j.tecto.2022.229593.

Wechsler, N., Rockwell, T.K., and Klinger, Y., 2018, Variable slip-rate and slip-per-event on a plate boundary fault: The Dead Sea fault in northern Israel: Tectonophysics, v. 722, p. 210–226, doi:10.1016/j.tecto.2017.10.017.

Witter, R.C., Bender, A.M., Scharer, K.M., DuRoss, C.B., Haeussler, P.J., and Lease, R.O., 2021, Geomorphic expression and slip rate of the Fairweather fault, southeast Alaska, and evidence for predecessors of the 1958 rupture: Geosphere, v. 17, p. 711–738, doi:10.1130/GES02299.1.

Yuan, Z., Liu-Zeng, J., Wang, W., Weldon, R.J., Oskin, M.E., Shao, Y., Li, Z., Li, Z., Wang, P., and Zhang, J., 2018, A 6000-year-long paleoseismologic record of earthquakes along the Xorkoli section of the Altyn Tagh fault, China: Earth and Planetary Science Letters, v. 497, p. 193–203, doi:10.1016/j.epsl.2018.06.008.

Yun, L., Zhang, J., Wang, J., Yang, X., Qu, J., Zhang, B., and Zhao, H., 2020, Active deformation to the north of the Altyn Tagh Fault: Constraints on the northward growth of the northern Tibetan Plateau: Journal of Asian Earth Sciences, v. 198, p. 104312, doi:10.1016/j.jseaes.2020.104312.